Reply to Reviewer #4

We thank you for your time and efforts in reviewing our manuscript. We considered all comments and suggestions and provided our detailed point-by-point responses below.

Overall Evaluation:

I recommend major revision. In short, I am concerned about the use of two grid configurations to study secondary eyewall formation (SEF) in tropical cyclones. That a simulation with smaller grid spacing produces SEF vs the coarser simulation is not surprising considering other studies on the topic. However, grid spacing fundamentally impacts the nature of turbulence and convection, thereby making the investigation of SEF a more complex problem experimentally. I suggest fixing grid spacing and either a small ensemble approach or set of well designed sensitivity experiments. The paper does a nice job examining the formation of a moat in the control simulation, but it is not clear how valuable the coarser resolution experiment is in comparison for fundamentally understanding SEF. With a small ensemble, or sensitivity experiments with fixed grid spacing, assuming there's a wide enough variance in SEF properties, then more emphasis can be put into getting into the valuable questions on the importance of mesoscale and microphysical impacts on moat formation, descending inflow jets, etc in SEF. At the moment, it is difficult to determine whether the current manuscript adds to our existing knowledge of SEF and moat formation.

Reply:

Based on your suggestions, we conducted a set of sensitivity experiments by changing the microphysics schemes with **a fixed grid spacing of 333 m** with limited computing resources in the limited time. The microphysics schemes used are WSM6 (CTL), WDM6, Thompson, and Lin (Fig. R4.1). It shows that the SEF occurs in simulations with different microphysics schemes, while the timing of the SEF differs.

In WDM6, the inner-eyewall convection does not develop vigorously from 20 h to 30 h. After 30 h, the inner-eyewall convection develops vigorously with strong eyewall updrafts shown in Fig. R4.1f. Thus, the SEF occurs around 48 h, which is 16-h later than that in WSM6. In Thompson and Lin, although the inner-eyewall updrafts

are stronger than that in WSM6, the SEF occurs later than that in WSM6 due to different inner-eyewall structures. Figures R4.1c-d and R4.1g-h show that the inner-eyewall expands from 24 h to 48 h, leading to the large-sized eyewall in Thompson and Lin compared to that in WSM6. Therefore, the SEF occurs earlier in WSM6 than that in Thompson and Lin. The horizontal distributions of the radar reflectivity at heights of 1, 3, 5, and 7 km at selected times in Thompson (Fig. R4.2) and Lin (Fig. R4.3) also show that the SEF occurs when the inner-eyewall convection becomes more compacted. It indicates that a large-sized eyewall with expanding and vigorous eyewall convection below the height of 7 km is not conducive to the generation of subsidence in the moat area. The sensitivity tests support our results by showing that the SEF occurs when the inner-eyewall updrafts are stronger, and the inner-eyewall convection is compacted.

Moreover, we think that the effects of grid spacing on the turbulence and convection can be reflected, to some extent, by the evolution of the eyewall convection. And the changes of the eyewall structures can be caused by any factor (like the different grid spacings, microphysics schemes, and initial vortex, etc.). The purpose of our study is to investigate the possible effects of the structural changes of the inner eyewall on the formation of the moat and the secondary eyewall, while understanding why eyewall structure differs to any factor is beyond the scope of our current study. Your suggestions have inspired us to do more research to understand how different microphysics schemes work on the SEF and to investigate the reliability of the microphysics schemes on the SEF.

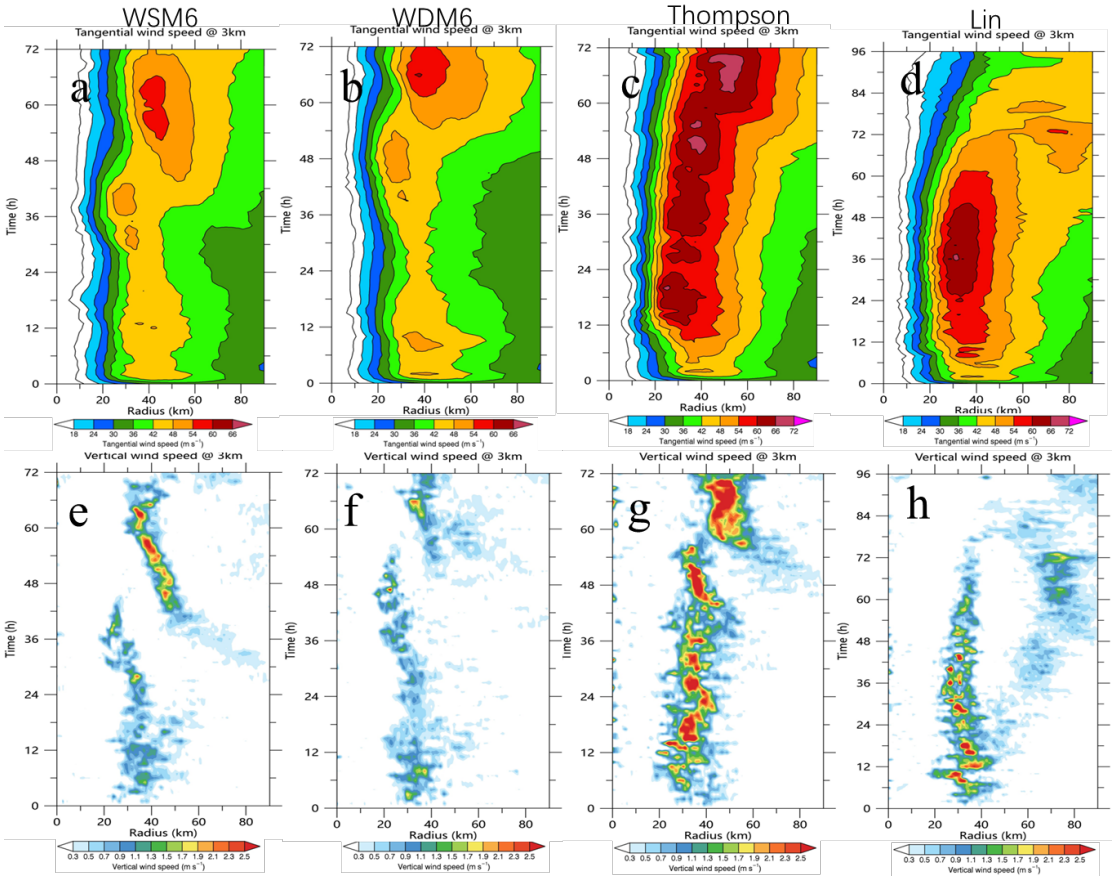

Figure R4.1 Radius-time cross-sections of the azimuthal mean (a-d) tangential wind (m s^{-1}) and (e-h) vertical motion (m s^{-1}) at z = 3 km for (a, e) WSM6, (b, f) WDM6, (c, g) Thompson, and (d, h) Lin.

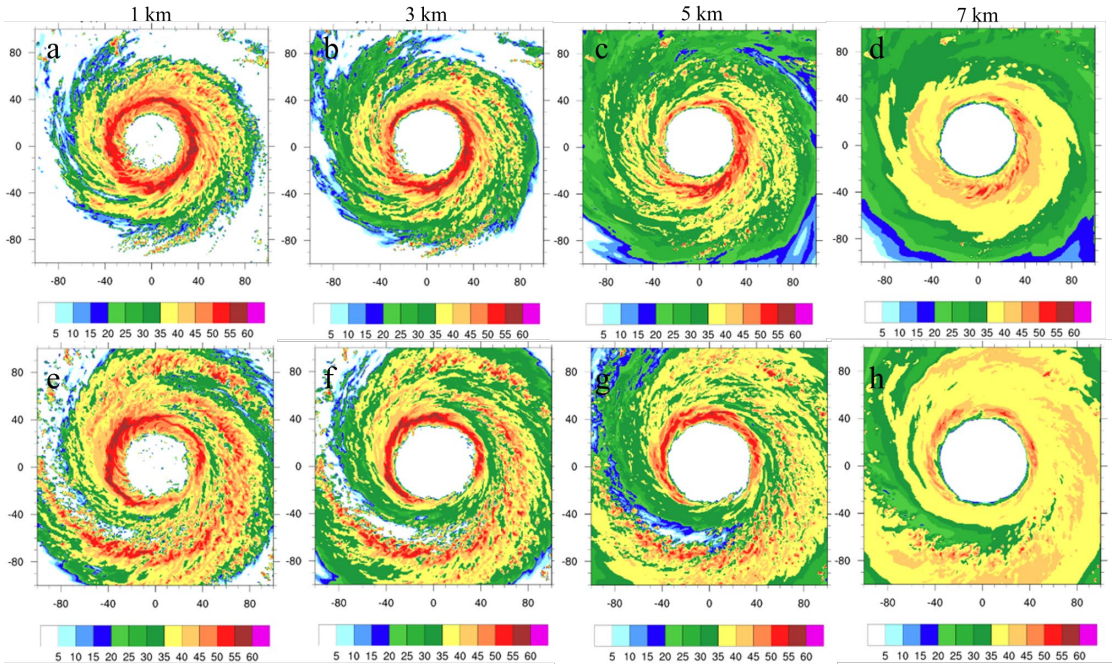

Figure R4.2 Horizontal distributions of the radar reflectivity at (a, e) 1-km, (b, f) 3-km, (c, g) 5-km, and (d, h) 7-km height at (a-d) 32 h and (e-h) 48 h in Thompson.

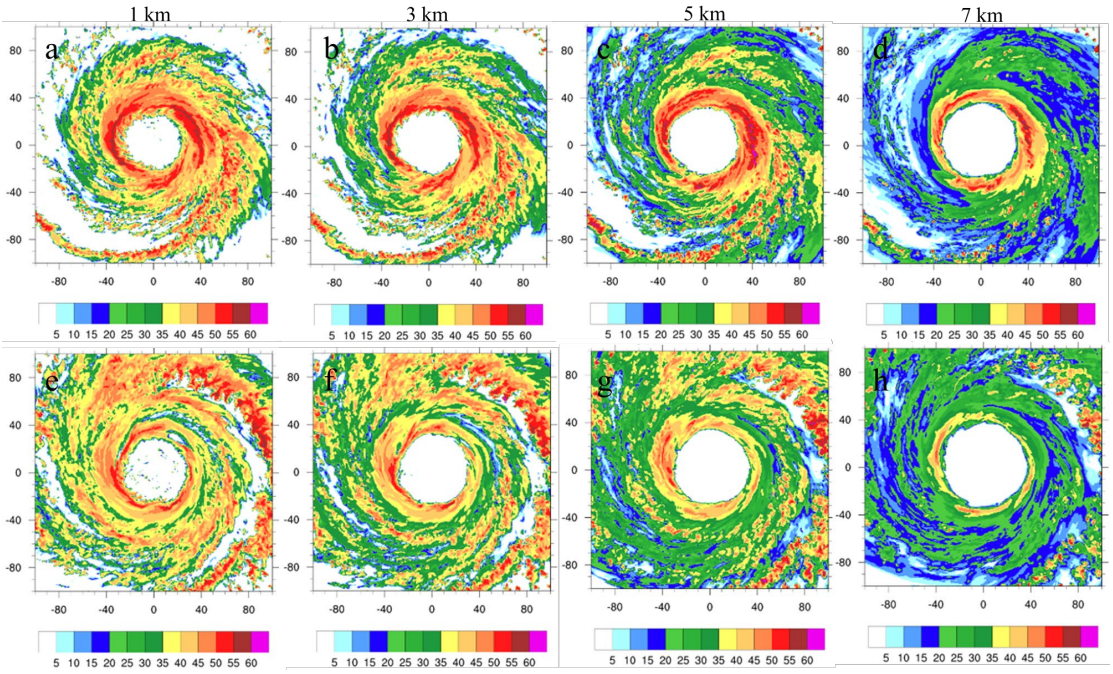

Figure R4.3 Horizontal distributions of the radar reflectivity at (a, e) 1-km, (b, f) 3-km, (c, g) 5-km, and (d, h) 7-km height at (a-d) 32 h and (e-h) 48 h in Lin.